ADVANCES IN ATMOSPHERIC SCIENCES, VOL. 32, SEPTEMBER 2015, 1208–1216

Three-type MJO Initiation processes over the Western Equatorial Indian Ocean

MEI Shuangli[1,2], Tim LI[*3,4], and CHEN Wen[1]

[1]*Center for Monsoon System Research, Institute of Atmospheric Physics, Chinese Academy of Sciences, Beijing,* 100029

[2]*University of Chinese Academy of Sciences, Beijing* 100049

[3]*International Laboratory on Climate and Environment Change and Key Laboratory of Meteorological Disaster of Ministry of Education, Nanjing University of Information Science and Technology, Nanjing* 210044

[4]*International Pacific Research Center, Department of Meteorology, School of Ocean and Earth Science and Technology, University of Hawaii at Manoa, Honolulu, Hawaii* 96822, *USA*

(Received 12 September 2014; revised 10 February 2015; accepted 16 February 2015)

ABSTRACT

Thirty strong Madden–Julian Oscillation (MJO) events in boreal winter 1982–2001 are selected to investigate the triggering processes of MJO convection over the western equatorial Indian Ocean (IO). These MJO events are classified into three types, according to their dynamic and thermodynamic precursor signals *in situ*. In Type I, a remarkable increase in low-level moisture occurs, on average, 7 days prior to the convection initiation. This low-level moistening is mainly due to the advection of the background mean moisture by easterly wind anomalies over the equatorial IO. In Type II, lower-tropospheric ascending motion anomalies develop, on average, 4 days prior to the initiation. The cause of this ascending motion anomaly is attributed to the anomalous warm advection, set up by a suppressed MJO phase in the equatorial IO. In Type III, there are no clear dynamic and thermodynamic precursor signals *in situ*. The convection might be triggered by energy accumulation in the upper layer associated with Rossby wave activity fluxes originated from the midlatitudes.

Key words: MJO, Indian Ocean, dynamic precursor signal, thermodynamic precursor signal

Citation: Mei, S. L., T. Li, and W. Chen, 2015: Three-type MJO Initiation processes over the Western Equatorial Indian Ocean. *Adv. Atmos. Sci.*, **32**(9), 1208–1216, doi: 10.1007/s00376-015-4201-0.

1. Introduction

Madden–Julian Oscillation (MJO) is a dominant atmospheric low-frequency mode in the tropics. With a typical planetary zonal scale and a 20–90-day period, MJO convective anomalies are often triggered in the western equatorial Indian Ocean (WEIO), and then propagate eastward along the equator to near the dateline (Lau and Chan, 1985; Knutson and Weickmann, 1987; Rui and Wang, 1990). The MJO is a major source of predictability for extended-range (10–30-day) weather prediction. However, many operational centers around the world suffer from prediction barrier problems at this range. Currently, as many operational forecast centers participate in subseasonal-to-seasonal forecast (S2S) projects, a key issue that these centers face is whether or not their operational models are able to successfully simulate and predict MJO initiation and subsequent evolution. Therefore, further exploration and understanding of MJO initiation and propagation issues are urgently needed.

Previous studies suggest that MJO convection can be triggered by a tropical and an extratropical process. The tropical process includes the discharge–recharge of local moisture (Bladé and Hartmann, 1993; Kemball-Cook and Weare, 2001), radiation–convection feedback (Hu and Randall, 1994), circumnavigation of convective coupled Kelvin waves that travel around the global equatorial regions (Lau and Peng, 1987; Hendon, 1988; Wang and Li, 1994), downstream forcing of Rossby waves associated with preceding suppressed phases of MJO in the eastern equatorial Indian Ocean (EEIO) (Matthews, 2000; Seo and Kim, 2003; Jiang and Li, 2005; Zhao et al., 2013), and delayed sea surface temperature feedback (Li et al., 2008).

The extratropical process is also an important mechanism for MJO initiation. The forcing from midlatitude perturbations propagates southward and equatorward (Hsu et al., 1990; Bladé and Hartmann, 1993; Matthews and Kiladis, 1999; Pan and Li, 2008; Ray et al., 2009). For example, Kiladis and Weickmann (1992) suggested that Rossby wave trains might propagate into the tropics from extratropical regions to trigger MJO convection. Matthews (2008) reported observations of enhanced Rossby wave activity between 10°N and 30°N, which led the convection onset of successive MJO events over the African and Indian Ocean (IO) regions. In addition, a case study by Ray et al. (2009) showed that equatorward momentum transport from the midlatitudes

* Corresponding author: Tim LI
Email: timli@hawaii.edu

might contribute to the generation of a low-level westerly that leads to MJO initiation. Wang et al. (2012) showed that subtropical cold surges could cause MJO convection initiation.

Many previous studies of MJO initiation were based on case studies or idealized numerical modeling. Recently, Zhao et al. (2013) showed, from a composite analysis of 20 years of observational data, that both the tropical lower-tropospheric moisture accumulation in the western IO and midlatitude wave processes are important. Ling et al. (2013) suggested that large-scale signals such as low-level easterly anomalies, surface pressure anomalies, and negative temperature anomalies from the middle to upper layers over the IO may distinguish between MJO and non-MJO events prior to their initiation. Straub (2012) found that 850 hPa easterly anomalies led by about 10 days before the convection onset of the primary MJO.

By examining individual cases of the same 20-year period as in Zhao et al. (2013), we noticed that individual MJO events experienced different precursor signals and thus different initiation processes. This motivated us to investigate individual MJO events, in order to understand what the different predecessors are and what their corresponding triggering processes involve. Accordingly, the present study investigates specific MJO initiation precursors and processes by examining each individual MJO event through diagnosis of a reanalysis dataset. The aim is then to try to elicit information on the commonalities and differences of theses samples, ultimately to reveal whether or not the extratropical forcing is independent of the tropical forcing. The outline of the paper is as follows: Section 2 introduces the datasets and methods used in the study. Section 3 presents the MJO initiation precursors and their respective triggering processes. A conclusion and discussion are given in section 4.

2. Data and methodology

2.1. *Data*

This study is based on ERA-40 reanalysis datasets (Uppala et al., 2005) and outgoing longwave radiation (OLR) datasets (Liebmann and Smith, 1996) derived from the European Centre for Medium-Range Weather Forecast (ECMWF) and the National Oceanic and Atmospheric Administration (NOAA) respectively, both with a 2.5° spatial resolution. Our analysis focuses on the same 20-yr period (1 January 1982 to 31 December 2001) northern winter (November–April) season as in Zhao et al. (2013). To examine the precursor SST signal, we use the Global Ocean Data Assimilation System (GODAS) pentad outputs of ocean temperature at the first layer (5 m), which has a resolution of $1^\circ \times 1^\circ$ that increases to $1/3^\circ$ in the north–south direction within 10° of the equator (Saha et al., 2006).

2.2. *Moisture and heat budgets diagnosis*

The intraseasonal moisture and heat budget below are performed to understand the cause of low-level moisture increase and anomalous ascending motion generation before MJO convection onset. They are derived from the temperature and specific humidity tendency equations (Yanai et al., 1973) by applying a 20–90-day band-pass Lanczos filter:

$$\left(\frac{\partial q}{\partial t}\right)' = (-\boldsymbol{V}\cdot\nabla q)' - \left(\omega\frac{\partial q}{\partial p}\right)' - \left(\frac{Q_2}{L}\right)', \quad (1)$$

$$\left(\frac{\partial T}{\partial t}\right)' = (-\boldsymbol{V}\cdot\nabla T)' + \left(\omega\frac{RT}{c_p p} - \omega\frac{\partial T}{\partial p}\right)' + (Q_1/c_p)', \quad (2)$$

where c_p represents the specific heat at constant pressure, R the gas constant, ∇ the horizontal gradient operator, L the latent heat of condensation, t time, p pressure, T temperature, q specific humidity, $\boldsymbol{V}$ the horizontal velocity vector, ω the vertical p-velocity, Q_1 diabatic heating, and Q_2 the atmospheric apparent moisture sink (Zhao et al., 2013). In addition, $(\,)'$ denotes the 20–90-day intraseasonal component.

Before conducting the moisture and heat budget analyses, variables including $\boldsymbol{V}, \omega, q$ and T are decomposed into three components: a 20-day high-pass filtered component (synoptic-scale disturbances); an intraseasonal (20–90-day filtered) component (MJO); and a 90-day low-pass filtered component (LFBS, low-frequency background state) (Hsu and Li, 2012). For example, the variable X, which is used to represent $\boldsymbol{V}$, ω, q or T, may be decomposed into

$$X = \overline{X} + X' + X^* , \quad (3)$$

where an overbar, a prime, and an asterisk represent the LFBS, MJO, and high-frequency component, respectively.

2.3. *Phase-independent wave activity flux*

To show the extratropical forcing effect on the MJO initiation, a wave activity flux is examined (Takaya and Nakamura, 2001; Zhao et al., 2013):

$$W = \frac{1}{2|\overline{U}|}\begin{pmatrix} \overline{u}(\psi_x'^2 - \psi'\psi'_{xx}) + \overline{v}(\psi'_x\psi'_y - \psi'\psi'_{xy}) \\ \overline{u}(\psi'_x\psi'_y - \psi'\psi'_{xy}) + \overline{v}(\psi_y'^2 - \psi'\psi'_{yy}) \end{pmatrix}, \quad (4)$$

where a bar and a prime represent the LFBS and the intraseasonal anomaly, W is the horizontal wave activity flux, u and v are zonal and meridional wind velocity, respectively, and ψ is the streamfunction (Zhao et al., 2013).

3. Precursor signals associated with Three-type initiation processes

The common features associated with MJO initiation during the 20-yr (1982–2001) northern winter period were examined by Zhao et al. (2013). Here, we focus on precursor signals associated with individual MJO events. Zhao et al. (2013) employed a regional EOF analysis method, with its first principal component amplitude more than one standard deviation as a criterion in selecting relatively strong MJO events. Using this method, a total of 55 cases are selected. The disadvantage of this method is that it includes local non-propagating or westward-propagating events. To overcome this problem, an objective method, carried out in a way similar to that of Rui and Wang (1990), is employed to select

strong, and the most representative, MJO events that formed over the WEIO. Firstly, a time–longitude diagram of the 20–90-day filtered OLR anomaly averaged over 10°S and 10°N is plotted. Then, MJO events are selected based on the time–longitude diagram using the following three criteria: (1) a contour line of negative OLR anomalies of -5 W m^{-2} must appear continuously from the WEIO ($\sim$60°E) to the western Maritime Continent ($\sim$100°E). This constraint ensures continuous eastward propagation of the MJO over the IO. (2) The maximum strength of the negative OLR anomaly over the equatorial IO exceeds -25 W m^{-2} (this lower limit is based on the standard deviation of OLR anomalies over the equatorial Indian Ocean and is applied to ensure that only strong MJO cases are selected). (3) At least 50% of the time span of the MJO event appears during the period from 1 November to 30 April of the following year. Using this criterion, we obtain 30 strong, continuous eastward-propagating MJO events that occurred during 1982–2001 and initiated over the WEIO. Among them, 23 events overlap with those of Zhao et al. (2013).

The information for all the selected individual MJO events is given in Table 1. For each event, the initiation region is determined according to the time–longitude diagram, following Zhao et al. (2013). Once the initiation region is determined, a box (at least $10^\circ \times 10^\circ$) averaged time series of the intraseasonal OLR anomaly is plotted, and the initiation date is then determined based on the OLR transition from positive to negative values (see Fig. 1a for an example). The vertical profiles of 20–90-day filtered key atmospheric variables such as vertical velocity, specific humidity and temperature are then examined.

Based on the examination of the aforementioned key dynamic and thermodynamic signals and their corresponding triggering processes before the initiation for each event, we put those MJO events with common characteristics together for analysis, and thus three types of initiation processes are identified. In the first type, PBL moisture anomalies significantly lead the convection onset. In the second type, lower-tropospheric ascending motion anomalies lead the convection initiation. In the third type, neither low-level specific humidity nor vertical motion lead the convection, but there is clear evidence of midlatitude Rossby wave activity flux convergence before the convection onset.

In the following, we investigate the common features associated with each of the three types of initiation processes. A composite analysis method was applied to each type, with a reference day (day 0) corresponding to the initiation date shown in Table 1. Therefore, day 0 represents the time of MJO convection initiation in the WEIO.

3.1. *Type I: PBL moisture-leading*

Seventeen out of thirty MJO events are identified as possessing the characteristic of robust PBL moisture leading MJO convection initiation. The left panel of Fig. 1 represents the composite time evolution of the intraseasonal OLR anomaly and vertical profiles of intraseasonal vertical velocity and specific humidity anomalies (Figs. 1a–c). Prior to the convection initiation, there are positive OLR and mid-tropospheric descending motion anomalies. On average, the PBL significant positive moisture anomalies lead the convection initiation by 7 days. The variance of the PBL moisture phase leading is 8.1, which implies a standard deviation of 2.9 days. Such a phase leading feature is statistically significant, exceeding the 95% confidence level. The moisture anomalies are initially confined to the lower level and then develop gradually upward into the upper troposphere (Fig. 1c). The low-level moisture increase could cause a convectively unstable stratification, resulting in the MJO convection initia-

Table 1. Information on the individual MJO events selected for each type, including case number and initiation date (in the format of year–month–day; for example, 19821214 corresponds to 14 December 1982).

Type I No.	Initiation date	Type II No.	Initiation date	Type III No.	Initiation date
1	19821214	1	19851207	1	19841017
2	19850125	2	19881024	2	19910405
3	19850331	3	19881228	3	19920311
4	19860416	4	19911115	4	19941011
5	19861011	5	19951008	5	19970131
6	19870405	6	19970417	6	20001105
7	19871129	7	19991116		
8	19871231				
9	19880305				
10	19891208				
11	19911210				
12	19930104				
13	19950321				
14	19950416				
15	19970320				
16	19990103				
17	20010115				

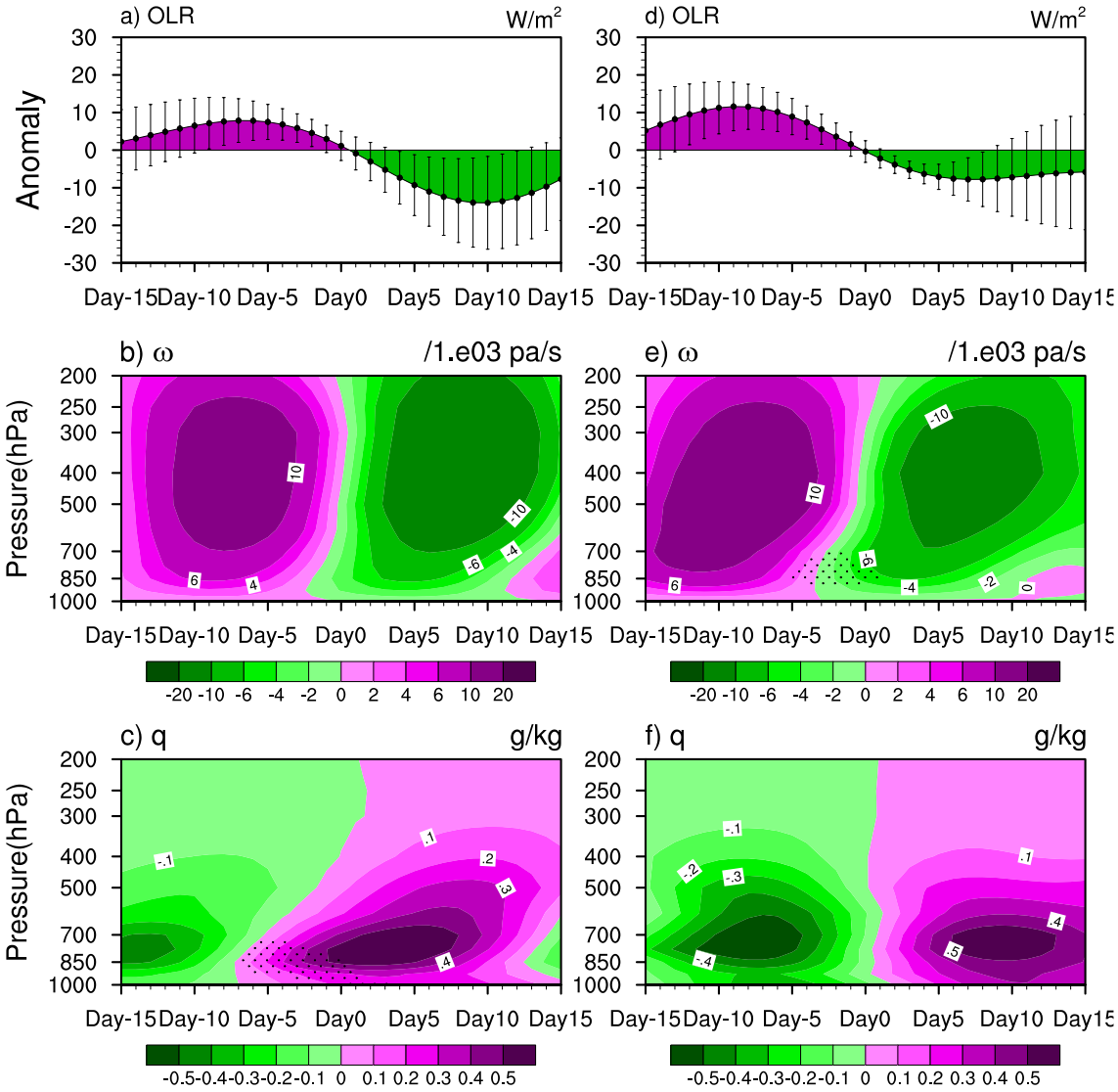

Fig. 1. (a, d) Composite evolutions of the intraseasonal OLR anomaly, (b, e) vertical profiles of intraseasonal vertical velocity, and (c, f) specific humidity for (a–c) Type and (d–f) Type II averaged over the initiation region for each individual event. Error bars represent the standard deviation of the OLR anomalies. Regions with statistical significance exceeding the 5% level are stippled.

tion. The onset of the shallow convection may be inferred from the vertical velocity profile from day −2 to day 0 (Fig. 1b), when anomalous ascending motion occurs primarily in the low level. After the initiation date, the ascending motion anomaly penetrates quickly into the upper troposphere, representing the onset of deep convection (Fig. 1b).

A key issue for the first type process is what contributes to the lower-tropospheric moisture increase before the convection initiation, when the large-scale descending motion is pronounced. To address this question, a vertically integrated (1000–700 hPa) moisture budget is diagnosed. Figure 2a shows the diagnosis result. The positive specific humidity tendency from day −7 to day 0 results from the positive horizontal specific humidity advection with the positive minimum standard deviation of the individual term. A further diagnosis of the horizontal specific humidity advection represents the fact that the major contribution arises from the advection of background mean specific humidity by the intraseasonal flow (term $-V' \cdot \nabla\overline{q}$) (Fig. 3a).

Figure 4 shows the composite of 1000–700 hPa integrated intraseasonal wind and background moisture fields averaged during the period from day −7 to day 0. Note that maximum mean specific humidity appears in the eastern IO and Maritime Continent, and mean moisture decreases toward the west. Moreover, the significant moisture field distributes over the equatorial IO regions. The intraseasonal flow field during day −7 to day 0 is characterized by easterly anomalies at the equator and two anticyclonic Rossby gyres off the equator in the tropical IO. The wind anomaly distribution is consistent with the Gill pattern (Gill, 1980) and is typically observed when the suppressed MJO phase is located over the EEIO. Further exploration of the intraseasonal OLR field confirms

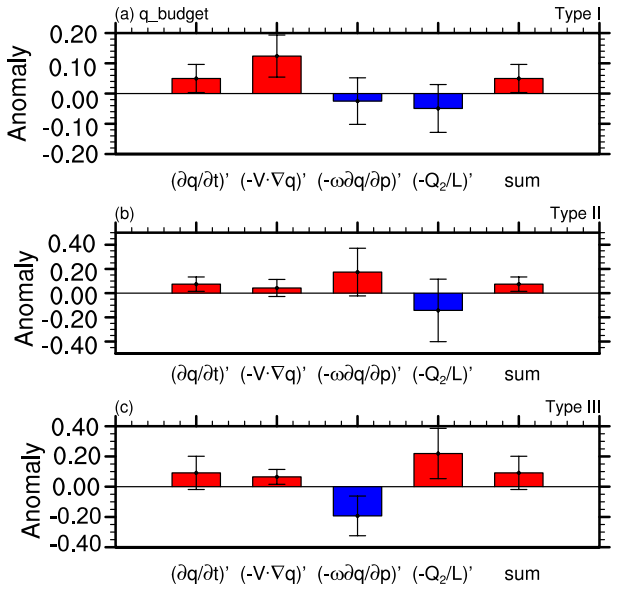

Fig. 2. Composites of vertically integrated (1000–700 hPa) intraseasonal moisture budget terms averaged over the initiation region of each individual event prior to the initiation time for (a) Type I (on average from day −7 to day 0), (b) Type II (on average from day −3 to day 0) and (c) Type III (on average from day −5 to day 0). Error bars represent the standard deviation among the sample members.

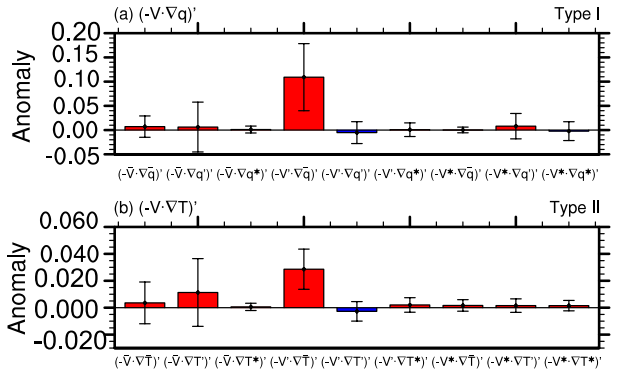

Fig. 3. Composites of individual components of the vertically integrated (1000–700 hPa) horizontal moisture advection term averaged during their respective initiation regions and periods for (a) Type I and (b) Type II events. Error bars represent the standard deviation among the sample members.

that a maximum positive OLR anomaly center associated with the MJO is located over the EEIO during this period (figure not shown). The intraseasonal flow advects the background high moisture westward, resulting in PBL moisture increases in the WEIO.

3.2. *Type II: PBL ascending-motion-leading*

Seven out of the thirty MJO events happened when significant PBL ascending motion anomalies led the convection initiation, while moisture anomalies did not. The right panel of Fig. 1 shows the composite time evolution of the intraseasonal OLR anomaly and the time–vertical sections of anomalous vertical motion and moisture fields. The ascending motion anomaly, which is significant at the 95% confidence level, occurs initially near the surface and develops gradually upward. On average, the PBL ascending motion leads the convection onset by 4 days (Figs. 1e and f), and the variance for the vertical motion phase-leading in Type II is 1.6. This implies a standard deviation of 1.3 days. Diagnosis of the low-level moisture budget during the period from day −3 to day 0 shows that the increased moisture is primarily caused by vertical advection, while the horizontal advection plays a minor role (Fig. 2b). A further analysis shows that the moistening due to vertical advection is mainly caused by the advection of mean moisture by anomalous ascending motion (figure not shown).

To understand the cause of the PBL ascending motion anomaly, we diagnose the lower-tropospheric heat budget, following Jiang and Li (2005). Figure 5b represents the composite of 1000–700 hPa integrated intraseasonal heat budget terms averaged during the period from day −4 to day 0. Compared with Fig. 5a, the budget result reveals that the horizontal temperature advection is a major term that is offset largely by the adiabatic cooling term, which is associated with vertical motions. In other words, the negative adiabatic heating, representing the cooling of the atmosphere induced by the ascending motion anomaly, is compensated by the anomalous horizontal warm advection. The temperature tendency term and the diabatic term are much smaller, and can be, to the first order of approximation, neglected. The result suggests that the PBL ascending motion is caused by the anomalous horizontal warm advection. This warm advection effect acts in a similar way to the traditional omega equation in a quasi-geostrophic framework (Holton, 2004).

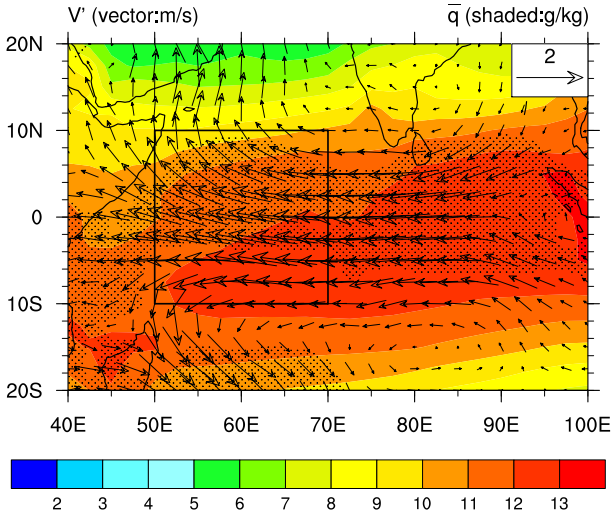

Fig. 4. Composites of 1000–700 hPa integrated intraseasonal wind and background mean specific humidity fields averaged during the initiation period (day −7 to day 0). The black box indicates the average initiation region (10°S–10°N, 50°–70°E) for Type I events. Regions with statistical significance exceeding the 5% level are stippled.

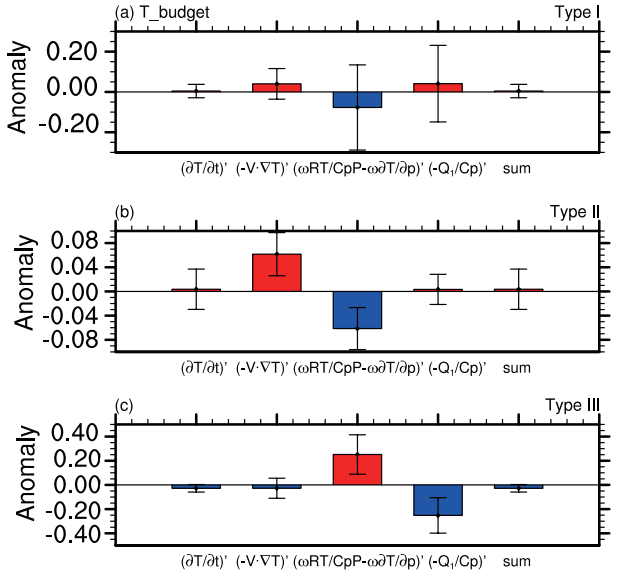

Fig. 5. Composites of 1000–700 hPa integrated intraseasonal heat budget terms averaged over their respective initiation regions and periods for (a) Type I, (b) Type II and (c) Type III events. Error bars represent the standard deviation of the sample members.

To further examine the source of the anomalous horizontal warm advection, each component of the horizontal temperature advection (Fig. 3b) is calculated. It is found that the largest contributor is the advection of LFBS mean temperature by intraseasonal flow. Figure 6 represents the spatial distribution of vertically integrated intraseasonal wind and background temperature fields averaged during the period of day −4 to day 0. Whereas maximum mean temperature appears over the EEIO, the MJO flow prior to the initiation is dominated by anomalous easterlies at the equator and anticyclonic flow to the south of the equator. The anomalous lower-tropospheric circulation is associated with a positive OLR anomaly centered over the tropical central IO (figure not shown). The anomalous easterly flow, which is statistically significant (exceeding the 95% confidence level), advects the background high temperature westward, leading to anomalous warm temperature advection, which induces anomalous ascending motion over the initiation region.

Another possible mechanism in generating PBL vertical motion is through SST forcing, in which warm SST anomalies could cause a PBL convergence via the change of PBL temperature and pressure fields (Lindzen and Nigam, 1987). The examination of the local intraseasonal SSTA field shows that for three (four) out of seven MJO events, there are positive (negative) precursor SSTA signals over the initiation region (figure not shown). This mixed SSTA condition implies that the ocean surface condition is not critical for generating the anomalous ascending motion. In contrast, the anomalous warm advection appears in all seven Type II events, implying that it plays a critical role in triggering anomalous ascending motion prior to MJO initiation.

3.3. *Type III: Neither PBL moisture-nor ascending-motion-leading*

In contrast to the first two types of initiation processes, there are no obvious local dynamic and thermodynamic precursor signals in Type III. A total of six events are identified for this type. Figure 7 shows the composite time evolution of the intraseasonal OLR anomaly, vertical motion, and moisture profiles for Type III. During the period of day −5 to day 0, descending motions and negative moisture anomalies appear over the initiation region in the low level (from 1000 to 700 hPa). Compared with Type I and Type II, it is apparent that the moisture tendency is positive, and the PBL moistening can be mainly attributed to the apparent moisture source term $(-Q^2/L)$ (Fig. 2c). The heat budget result shows that the descending-motion-induced adiabatic warming is offset by the diabatic heating. The horizontal temperature advection, on the other hand, is very small (Fig. 5 c).

Although no robust tropical precursor signals can be found (Figs. 7b and c), there are clear midlatitude signals prior to Type III MJO convection onset. Figure 8 represents the composite upper-tropospheric (200 hPa) streamfunction anomaly pattern prior to the initiation date (averaged from day −5 to day 0). It is clear that the streamfunction anomalies display a clear wave train pattern, particularly in the Southern Hemisphere, with positive anomaly centers located in the western South Atlantic and South Africa, and negative anomaly centers in the southwestern South Atlantic and southeast South Atlantic. The 200 hPa wave activity flux field exhibits an equatorward wave energy dispersion characteristic. In the midlatitudes, there are pronounced eastward wave activity fluxes, which turn equatorward and converge onto the tropical IO (Fig. 8).

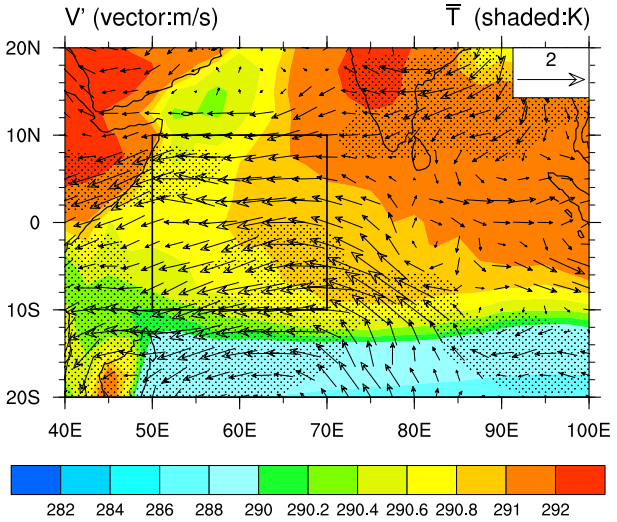

Fig. 6. Composite patterns of 1000–700 hPa integrated intraseasonal wind and background temperature fields averaged during the initiation period (day −4 to day 0) for Type II events. The black box indicates the average initiation region (10°S–10°N, 50°–70°E) for Type II events. Regions with statistical significance exceeding the 5% level are stippled.

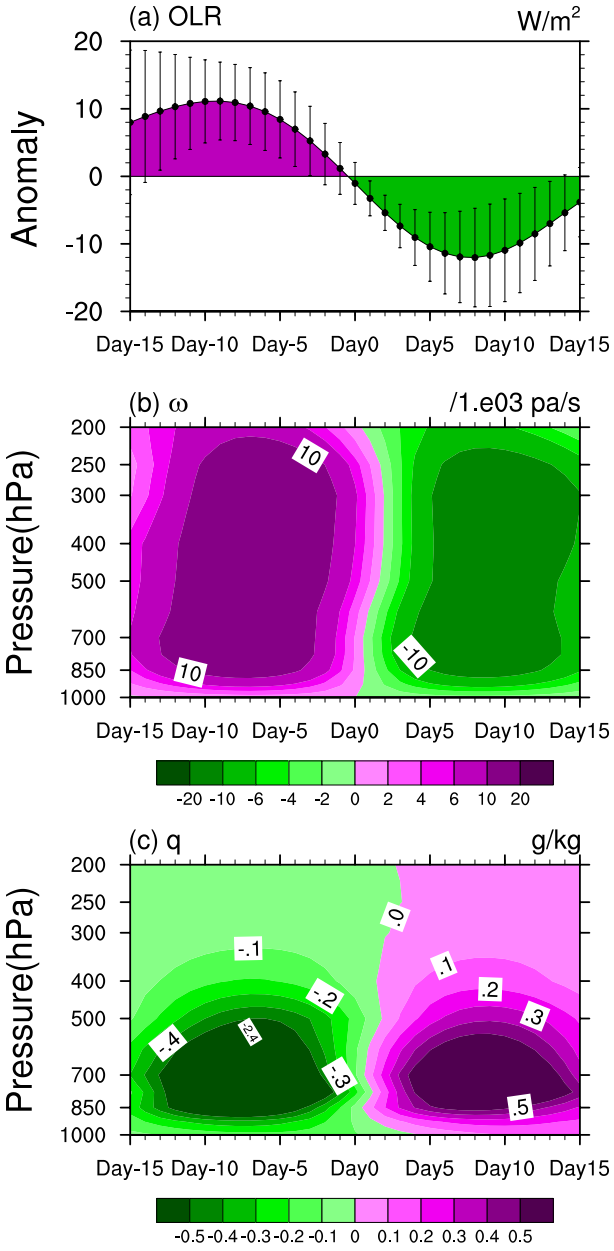

Fig. 7. (a–c) As in Fig. 1a–c but for Type III events, calculated over their respective initiation regions. Error bars represents the standard deviation of the OLR anomalies among the sample members.

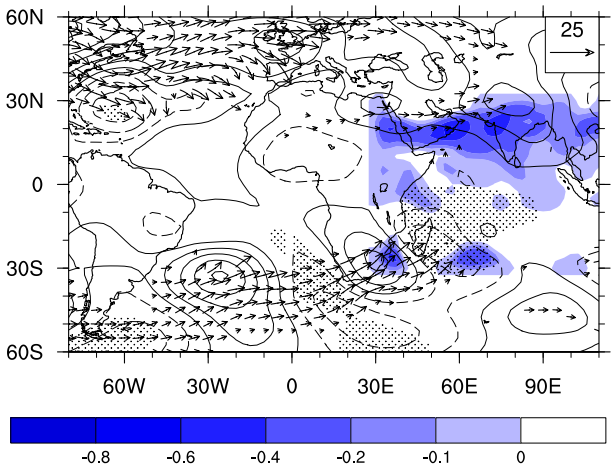

Fig. 8. Composite patterns of the 20–90-day filtered streamfunction anomaly (contours, $m^2\ s^{-2}$), Rossby wave activity flux (vectors, $m^2\ s^{-2}$), and flux divergence (color shading, 10^{-5} $m\ s^{-2}$; only negative values in the tropical IO are shaded) at 200 hPa averaged from day −5 to day 0 for Type III events. Arrows with absolute values of wave flux component greater than 4 $m^2\ s^{-2}$ are plotted. Regions with statistical significance exceeding the 5% level are stippled for the streamfunction anomaly field.

4. Conclusion and discussion

In the present reported study, the early signals and initiation processes relating to each one of a set of individual MJO events over the WEIO in winter are investigated through diagnosis of a 20-yr ERA-40 reanalysis dataset. Thirty strong, continuous eastward-propagating MJO events are selected for analysis. These events are classified into three types according to their precursor local moisture and vertical motion signals.

For Type I, MJO initiation is characterized by a PBL moisture-leading process. Seventeen events are identified for this type. The analysis shows that a notable increase of the lower-tropospheric specific humidity occurs 7 days before MJO convection onset. The increase of lower-tropospheric moisture induces a convectively unstable stratification, leading to the MJO convection onset over the WEIO. The diagnosis of the lower-level specific humidity budget shows that the moistening is induced mainly by the advection of the mean moisture by the MJO flow. The anomalous wind is a part of the Rossby wave response to a preceding MJO suppressed phase with a heating anomaly over the EEIO.

For Type II, MJO initiation is characterized by a phase leading of lower-tropospheric ascending motion. Seven events are identified for this type. The analysis shows that significant development of the lower-tropospheric ascending motion occurs 4 days prior to MJO convection onset. The ascending motion anomalies advect atmospheric moisture upward, promoting latent heat release and triggering MJO convection. A diagnosis of the lower-level heat budget indicates that anomalous warm horizontal advection prior to the convection initiation is a primary factor triggering the ascending motion anomaly. Further diagnosis suggests that the warm advection is mainly due to the advection of the background mean temperature by equatorial easterly anomalies in response to a positive OLR anomaly in the equatorial IO.

For Type III, no clear precursor moisture and ascending motion signals are found *in situ*. The forcing arises primarily from midlatitude perturbations. Six events are identified. The composite analysis shows that there are robust Rossby wave train signals in the upper troposphere (with alternate cyclonic and anticyclonic circulation) extending from the midlatitudes to the tropical IO a few days prior to Type III MJO initiation. The upper-tropospheric wave activity fluxes point toward the

tropical IO, with a flux convergence occurring there. The result implies that midlatitude Rossby wave energy accumulation may have an effect on the triggering of MJO convection.

Compared with the composite result of Zhao et al. (2013), who showed common precursor features of MJO initiation, the current analysis suggests three different types of initiation characteristics among individual events within the 20 year period. Through event-by-event examination, we have classified the MJO initiation scenarios into three types based on local dynamic and thermodynamic precursor signals. We believe that such a classification is helpful for operational application to identify and predict individual MJO initiation events.

However, it is worth mentioning that such a classification has its limitations. For example, Types I and II do not exclude the midlatitude wave impact. In fact, we note that eight out of seventeen Type I events and two out of seven Type II events involve the midlatitude wave energy dispersion effect. This indicates that during the initiation of these MJO events, both tropical and extratropical processes might work together. For these mixed events, it is important to further reveal the relative roles of the tropical and extratropical processes through idealized numerical experiments that isolate each of the processes. We intend to carry out this work in the near future. For Type III, on the other hand, the midlatitude wave process seems to be working alone, since key dynamic and thermodynamic precursor signals in the tropical region were not found.

Another issue is how the current findings relate to successive and primary events (Matthews, 2008). It is likely that Type I events are more like successive cases, since they are preceded by low-level easterly anomalies in the equatorial IO induced by a preceding suppressed-phase MJO event (Fig. 4, also see Zhao et al., 2013). Type II and III cases, on the other hand, are more likely primary events, since they are triggered either by extratropical forcing or heating anomalies not related to preceding MJO events. More in-depth observational analyses and numerical modeling studies are needed to reveal the origin of the precursor heating and circulation anomalies associated with Type II events and specific processes through which midlatitude waves affect tropical convection.

Acknowledgements. This research was supported by the China National 973 Project Grant No. 2015CB453200), the National Natural Science Foundation of China Grant Nos. 41475084 and 41230527, the Office of Naval Research Grant No. N00014-1210450, and the International Pacific Research Center (IPRC) sponsored by the Japan Agency for Marine-Earth Science and Technology. The School of Ocean and Earth Science and Technology contribution number is 9293, the IPRC contribution number is 1106, and Earth Science Modeling Center contribution number 039. We wish to thank the reviewers for their valuable suggestions, which helped to improve the manuscript.

REFERENCES

Bladé, I., and D. L. Hartmann, 1993: Tropical intraseasonal oscillations in a simple nonlinear model. *J. Atmos. Sci.*, **50**, 2922–2939, doi: 10.1175/1520-0469(1993)050<2922:TIOIAS>2.0.CO;2.

Gill, A. E., 1980: Some simple solutions for heat-induced tropical circulation. *Quart. J. Roy. Meteor. Soc.*, **106**, 447–462, doi: 10.1002/qj.49710644905.

Hendon, H. H., 1988: A simple model of the 40-50 day oscillation. *J. Atmos. Sci.*, **45**, 569–584, doi: 10.1175/1520-0469(1988)045<0569:ASMOTD>2.0.CO;2.

Holton, J., 2004: *An Introduction to Dynamic Meteorology*. 4th ed., Academic Press, 535 pp.

Hsu, H.-H., B. J. Hoskins, and F.-F. Jin, 1990: The 1985/86 intraseasonal oscillation and the role of the extratropics. *J. Atmos. Sci.*, **47**, 823–839, doi: 10.1175/1520-0469(1990)047<0823:TIOATR>2.0.CO;2.

Hsu, P.-C., and T. Li, 2012: Role of the boundary layer moisture asymmetry in causing the eastward propagation of the Madden-Julian oscillation. *J. Climate*, **25**, 4914–4931, doi: 10.1175/JCLI-D-11-00310.1.

Hu, Q., and D. A. Randall, 1994: Low-frequency oscillations in radiative-convective systems. *J. Atmos. Sci.*, **51**, 1089–1099, doi: 10.1175/1520-0469(1994)051<1089:LFOIRC>2.0.CO;2.

Jiang, X.-A., and T. Li, 2005: Reinitiation of the boreal summer intraseasonal oscillation in the tropical Indian Ocean. *J. Climate*, **18**, 3777–3795, doi: 10.1175/JCLI3516.1.

Kemball-Cook, S. R., and B. C. Weare, 2001: The onset of convection in the Madden-Julian oscillation. *J. Climate*, **14**, 780–793, doi: 10.1175/1520-0442(2001)014<0780:TOOCIT>2.0.CO;2.

Kiladis, G. N., and K. M. Weickmann, 1992: Circulation anomalies associated with tropical convection during northern winter. *Mon. Wea. Rev.*, **120**, 1900–1923, doi: 10.1175/1520-0493(1992)120<1900:CAAWTC>2.0.CO;2.

Knutson, T. R., and K. M. Weickmann, 1987: 30–60 day atmospheric oscillations: Composite life cycles of convection and circulation anomalies. *Mon. Wea. Rev.*, **115**, 1407–1436, doi: 10.1175/1520-0493(1987)115<1407:DAOCLC>2.0.CO;2.

Lau, K.-M., and P. H. Chan, 1985: Aspects of the 40–50 day oscillation during the northern winter as inferred from outgoing longwave radiation. *Mon. Wea. Rev.*, **113**, 1889–1909, doi: 10.1175/1520-0493(1985)113<1889:AOTDOD>2.0.CO;2.

Lau, K.-M., and L. Peng, 1987: Origin of low-frequency (intraseasonal) oscillations in the tropical atmosphere. Part I: Basic theory. *J. Atmos. Sci.*, **44**, 950–972, doi: 10.1175/1520-0469(1987)044<0950:OOLFOI>2.0.CO;2.

Li, T., F. Tam, X. H. Fu, T. J. Zhou, and W. J. Zhu, 2008: Causes of the intraseasonal SST variability in the tropical Indian Ocean. *Atmos. Oceanic Sci. Lett.*, **1**, 18–23.

Liebmann, B., and C. A. Smith, 1996: Description of a complete (interpolated) outgoing longwave radiation dataset. *Bull. Amer. Meteor. Soc.*, **77**, 1275–1277.

Lindzen, R. S., and S. Nigam, 1987: On the role of sea surface temperature gradients in forcing low-level winds and convergence in the tropics. *J. Atmos. Sci.*, **44**, 2418–2436, doi: 10.1175/1520-0469(1987)044<2418:OTROSS>2.0.CO;2.

Ling, J., C. D. Zhang, and P. Bechtold, 2013: Large-scale distinctions between MJO and Non-MJO convective initiation over the tropical Indian Ocean. *J. Atmos. Sci.*, **70**, 2696–2712, doi: 10.1175/JAS-D-13-029.1.

Matthews, A. J., 2000: Propagation mechanisms for the Madden-Julian Oscillation. *Quart. J. Roy. Meteor. Soc.*, **126**, 2637–2651, doi: 10.1002/qj.49712656902.

Matthews, A. J., 2008: Primary and successive events in the Madden-Julian oscillation. *Quart. J. Roy. Meteor. Soc.*, **134**, 439–453, doi: 10.1002/qj.224.

Matthews, A. J., and G. N. Kiladis, 1999: The tropical-extratropical interaction between high-frequency transients and the Madden-Julian oscillation. *Mon. Wea. Rev.*, **127**, 661–677, doi: 10.1175/1520-0493(1999)127<0661:TTEIBH>2.0.CO;2.

Pan, L.-L., and T. Li, 2008: Interactions between the tropical ISO and midlatitude low-frequency flow. *Climate Dyn.*, **31**, 375–388, doi: 10.1007/s00382-007-0272-7.

Ray, P., C. D. Zhang, J. Dudhia, and S. S. Chen, 2009: A numerical case study on the initiation of the Madden-Julian oscillation. *J. Atmos. Sci.*, **66**, 310–331, doi: 10.1175/2008JAS2701.1.

Rui, H. L., and B. Wang, 1990: Development characteristics and dynamic structure of tropical intraseasonal convection anomalies. *J. Atmos. Sci.*, **47**, 357–379, doi: 10.1175/1520-0469(1990)047<0357:DCADSO>2.0.CO;2.

Saha, S., and Coauthors, 2006: The NCEP climate forecast system. *J. Climate*, **19**, 3483–3517, doi: 10.1175/JCLI3812.1.

Seo, K. H., and K. Y. Kim, 2003: Propagation and initiation mechanisms of the Madden-Julian oscillation. *J. Geophys. Res.*, **108**, 4384, doi: 10.1029/2002JD002876.

Straub, K. H., 2012: MJO initiation in the real-time multivariate MJO index. *J. Climate*, **26**, 1130–1151, doi: 10.1175/JCLI-D-12-00074.1.

Takaya, K., and H. Nakamura, 2001: A formulation of a phase-independent wave-activity flux for stationary and migratory quasigeostrophic eddies on a zonally varying basic flow. *J. Atmos. Sci.*, **58**, 608–627, doi: 10.1175/1520-0469(2001)058<0608:AFOAPI>2.0.CO;2.

Uppala, S. M., and Coauthors, 2005: The ERA-40 re-analysis. *Quart. J. Roy. Meteor. Soc.*, **131**, 2961–3012, doi: 10.1256/qj.04.176.

Wang, B., and T. M. Li, 1994: Convective interaction with boundary-layer dynamics in the development of a tropical intraseasonal system. *J. Atmos. Sci.*, **51**, 1386–1400, doi: 10.1175/1520-0469(1994)051<1386:CIWBLD>2.0.CO;2.

Wang, L., K. Kodera, and W. Chen, 2012: Observed triggering of tropical convection by a cold surge: Implications for MJO initiation. *Quart. J. Roy. Meteor. Soc.*, **138**, 1740–1750, doi: 10.1002/qj.1905.

Yanai, M., S. Esbensen, and J.-H. Chu, 1973: Determination of bulk properties of tropical cloud clusters from large-scale heat and moisture budgets. *J. Atmos. Sci.*, **30**, 611–627, doi: 10.1175/1520-0469(1973)030<0611:DOBPOT>2.0.CO;2.

Zhao, C. B., T. Li, and T. J. Zhou, 2013: Precursor signals and processes associated with MJO initiation over the Tropical Indian Ocean. *J. Climate*, **26**, 291–370, doi: 10.1175/JCLI-D-12-00113.1.